



Mott Transition in VO₂ Revealed by Infrared Spectroscopy and Nano-Imaging

M. M. Qazilbash, *et al.*
Science **318**, 1750 (2007);
DOI: 10.1126/science.1150124

The following resources related to this article are available online at www.sciencemag.org (this information is current as of December 16, 2007):

Updated information and services, including high-resolution figures, can be found in the online version of this article at:

<http://www.sciencemag.org/cgi/content/full/318/5857/1750>

Supporting Online Material can be found at:

<http://www.sciencemag.org/cgi/content/full/318/5857/1750/DC1>

This article **cites 29 articles**, 3 of which can be accessed for free:

<http://www.sciencemag.org/cgi/content/full/318/5857/1750#otherarticles>

This article appears in the following **subject collections**:

Physics

<http://www.sciencemag.org/cgi/collection/physics>

Information about obtaining **reprints** of this article or about obtaining **permission to reproduce this article** in whole or in part can be found at:

<http://www.sciencemag.org/about/permissions.dtl>

material parameters, such as the viscosity, and scales quadratically with the wavelength of the optical pulses. It equals ~ 3.4 ns for our storage material, so that our current system is most appropriate for high-data-rate communication systems.

We use a short length of commercially available optical fiber and light pulses with a center wavelength around $1.55 \mu\text{m}$, which is in the middle of the telecommunication band (17). Fig. 2A shows the experimental results for storing and retrieving a single rectangular-shaped 2-ns-long data pulse using identical, 1.5-ns-long write and read pulses with peak powers of ~ 100 W. To the left of the dashed vertical line, the incident data pulse in the absence and presence of the write and read pulses is shown by the blue and green lines, respectively. The energy storage efficiency of the storage process is very high—equal to $\sim 66\%$ —indicating that we have faithfully encoded the optical pulse information onto the acoustic material excitation.

The data pulses are released from the fiber after a controllable storage time T_s by applying a read pulse, which converts the acoustic material excitation back to the optical domain. The curves to the right of the vertical dashed line are the observed retrieved pulses, where we have scaled them by a factor of 2 for clarity. For $T_s = 4$ ns, we obtain a readout energy efficiency of 25%, defined as the energy of the released pulse divided by the energy of the incident data pulse. For $T_s = 12$ ns, the storage time is equal to 6 pulse widths with an efficiency of 1.8%. These observations suggest that this method is useful for a class of high-speed, all-optical information processing applications, such as pulse correlation (18). Consistent with the discussion above, we see that the readout efficiency drops with increasing storage time as a result of the decay of the acoustic wave.

The fast rising and falling edges of the data pulse in the time domain contribute to its high-frequency content in the frequency domain. Thus, we hypothesize that the edges are not fully stored because the write-pulse spectrum is not broad enough to fully encompass the data-pulse spectrum; its spectrum is only slightly wider than the data-pulse spectrum. To test this hypothesis, we stored and retrieved a smoothed data pulse, as shown in Fig. 2B. In this case, the energy storage efficiency increases to 86% and the readout efficiencies are improved slightly ($\sim 29\%$ for $T_s = 4$ ns).

To verify the interpretation of our results, we have solved numerically the equations governing the interaction between the optical and acoustic waves in an optical fiber. The simulations (Fig. 2, C and D) are in good agreement with observations (17).

Fig. 3, A and B, shows our observations for the storage and retrieval of sequences of two and three data pulses, respectively. For clarity, we show only the input data pulses to

the left of the dashed vertical line and to the right we show the retrieved pulses scaled by a factor of 5. The light released from the fiber clearly replicates the input data stream with reasonable fidelity. Again, the numerical simulations (Fig. 3, C and D) are in good agreement with the observations (Fig. 3, A and B).

Our results demonstrate that coherent optical storage can be realized without the use of atomic spin coherence such as that used in EIT-based stored light. Longer storage times may be expected using materials with longer acoustic lifetimes, such as chalcogenide glass fibers ($\tau_B = 12$ ns for As_2Se_3 at a wavelength of $1.55 \mu\text{m}$) (19) or high-pressure gases ($\tau_B = 80$ ns for Xe at 140 atm and a wavelength of $1.55 \mu\text{m}$) (13). Also, the peak powers of the write and read pulses can be lowered substantially using fibers with a larger SBS gain coefficient (e.g., g_B for As_2Se_3 is 134 times as large as that of silica) (19) or smaller core sizes (i.e., smaller mode area). With such improvements, our method should be suitable for use in the buffering of information and for all-optical data processing such as correlation and convolution.

References and Notes

1. R. S. Tucker, P.-C. Ku, C. J. Chang-Hasnain, *J. Lightwave Technol.* **23**, 4046 (2005).
2. H. Lin, T. Wang, T. W. Mossberg, *Opt. Lett.* **20**, 1658 (1995).
3. M. Fleischhauer, S. F. Yelin, M. D. Lukin, *Opt. Comm.* **179**, 395 (2000).

4. C. Liu, Z. Dutton, C. H. Behroozi, L. V. Hau, *Nature* **409**, 490 (2001).
5. D. F. Phillips, A. Fleischhauer, A. Mair, R. L. Walsworth, M. D. Lukin, *Phys. Rev. Lett.* **86**, 783 (2001).
6. A. V. Turukhin et al., *Phys. Rev. Lett.* **88**, 023602 (2002).
7. M. D. Lukin, *Rev. Mod. Phys.* **75**, 457 (2003).
8. J. J. Longdell, E. Fraval, M. J. Sellars, N. B. Manson, *Phys. Rev. Lett.* **95**, 063601 (2005).
9. T. Chanelière et al., *Nature* **438**, 833 (2005).
10. C. W. Chou et al., *Nature* **438**, 828 (2005).
11. M. F. Yanik, W. Suh, Z. Wang, S. Fan, *Phys. Rev. Lett.* **93**, 233903 (2004).
12. Q. Xu, P. Dong, M. Lipson, *Nat. Phys.* **3**, 406 (2007).
13. R. W. Boyd, *Nonlinear Optics*, 2nd Ed. (Academic Press, San Diego, 2003), Ch. 9.
14. G. P. Agrawal, *Nonlinear Fiber Optics*, 3rd Ed. (Academic Press, San Diego, 2001), Ch. 9.
15. I. Y. Dodin, N. J. Fisch, *Phys. Rev. Lett.* **88**, 165001 (2002).
16. I. Y. Dodin, N. J. Fisch, *Opt. Commun.* **214**, 83 (2002).
17. Materials and methods are available as supporting material on Science Online.
18. R. Ramaswami, K. N. Sivarajon, *Optical Networks: A Practical Perspective* (Morgan Kaufmann, San Francisco, CA, 2002), Ch. 12.
19. K. F. Abedin, *Opt. Express* **13**, 10266 (2005).
20. We gratefully acknowledge the financial support from the Defense Advanced Research Projects Agency, Defense Sciences Office Slow-Light Program.

Supporting Online Material

www.sciencemag.org/cgi/content/full/318/5857/1748/DC1
Materials and Methods
Figs. S1 and S2
References

10 August 2007; accepted 23 October 2007
10.1126/science.1149066

Mott Transition in VO_2 Revealed by Infrared Spectroscopy and Nano-Imaging

M. M. Qazilbash,^{1*} M. Brehm,² Byung-Gyu Chae,³ P.-C. Ho,¹ G. O. Andreev,¹ Bong-Jun Kim,³ Sun Jin Yun,³ A. V. Balatsky,⁴ M. B. Maple,¹ F. Keilmann,² Hyun-Tak Kim,³ D. N. Basov¹

Electrons in correlated insulators are prevented from conducting by Coulomb repulsion between them. When an insulator-to-metal transition is induced in a correlated insulator by doping or heating, the resulting conducting state can be radically different from that characterized by free electrons in conventional metals. We report on the electronic properties of a prototypical correlated insulator vanadium dioxide in which the metallic state can be induced by increasing temperature. Scanning near-field infrared microscopy allows us to directly image nanoscale metallic puddles that appear at the onset of the insulator-to-metal transition. In combination with far-field infrared spectroscopy, the data reveal the Mott transition with divergent quasi-particle mass in the metallic puddles. The experimental approach used sets the stage for investigations of charge dynamics on the nanoscale in other inhomogeneous correlated electron systems.

One challenge of contemporary condensed matter physics is the understanding of the emergence of metallic transport in correlated insulators or Mott insulators in which, for example, a temperature change or chemical doping induces anomalous conducting phases (1). In such a correlated metal, the mobile charges experience strong competing interactions leading

to exotic phases, including the pseudogap state in cuprates and manganites, high-temperature superconductivity, charge stripes in cuprates, and even phase separation in some manganites and cuprates (1–8). In systems where multiple phases coexist on the nanometer scale, the dynamical properties of these individual electronic phases remain unexplored because methods appropriate to study charge

dynamics (transport, infrared/optical, and many other spectroscopies) lack the required spatial resolution. Scanning near-field infrared microscopy can circumvent this limitation (9–11). Specifically, we probed coexisting phases in the vicinity of the insulator-to-metal transition in vanadium dioxide (VO₂) at length scales down to 20 nm. This enabled us to identify an electronic characteristic of the Mott transition, namely divergent quasi-particle mass in the metallic puddles, which would otherwise have remained obscured in macroscopic studies that average over the coexisting phases in the insulator-to-metal transition regime.

One particular advantage of VO₂ for the study of electronic correlations is that the transition to the conducting state is initiated by increasing the temperature without the need to modify the stoichiometry. The salient features of the first-order phase transition that occurs at $T_c \approx 340$ K are the orders-of-magnitude increase in conductivity accompanied by a change in the lattice structure (1). Compared to the high-temperature rutile metallic (R) phase, the two main features that distinguish the lattice in the low-temperature monoclinic (M1) insulating phase are dimerization (charge-ordering) of the vanadium ions into pairs and the tilting of these pairs with respect to the *c* axis of the rutile metal. The experiments on VO₂ films (12, 13) reported here reveal a strongly correlated conducting state that exists within the insulator-to-metal transition region in the form of nanoscale metallic puddles. Electromagnetic response of these puddles separated by the insulating host displays the signatures of collective effects in the electronic system, including divergent optical effective mass and optical pseudogap. These findings, which were not anticipated by theoretical models, may also help to settle the decades-long debate (1, 14–20) on the respective roles played by the lattice and by the electron-electron correlations in the insulator-to-metal transition.

The gross features of the insulator-to-metal transition in VO₂ can be readily identified through the evolution of the far-field optical constants (13) obtained with use of spectroscopic ellipsometry and reflectance (Fig. 1). The insulating monoclinic phase ($T \leq 341$ K) displays a sizable energy gap of about 4000 cm⁻¹ (≈ 0.5 eV) in the dissipative part of the optical conductivity, $\sigma_1(\omega)$. The $T \geq 360$ K rutile metallic phase is characterized by a broad Drude-like feature in the optical conductivity, linear temperature dependence of resistivity, and an extremely short elec-

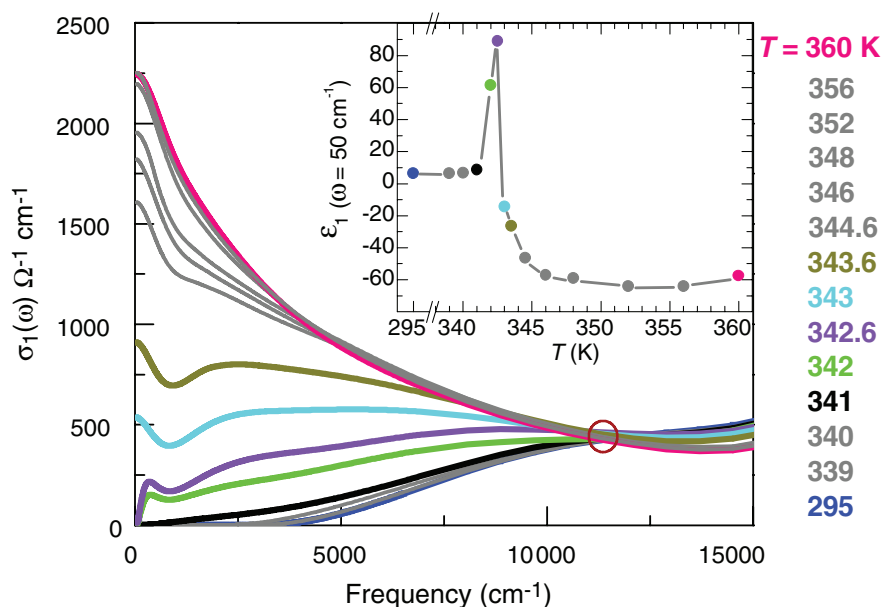


Fig. 1. The real part of the optical conductivity $\sigma_1(\omega) = \frac{\omega \epsilon_2(\omega)}{4\pi}$ of VO₂ is plotted as a function of frequency for various representative temperatures. The open circle denotes the isosbestic (equal conductivity) point for all spectra. (**Inset**) The temperature dependence of the real part of the dielectric function ϵ_1 in the low-frequency limit ($\omega = 50$ cm⁻¹).

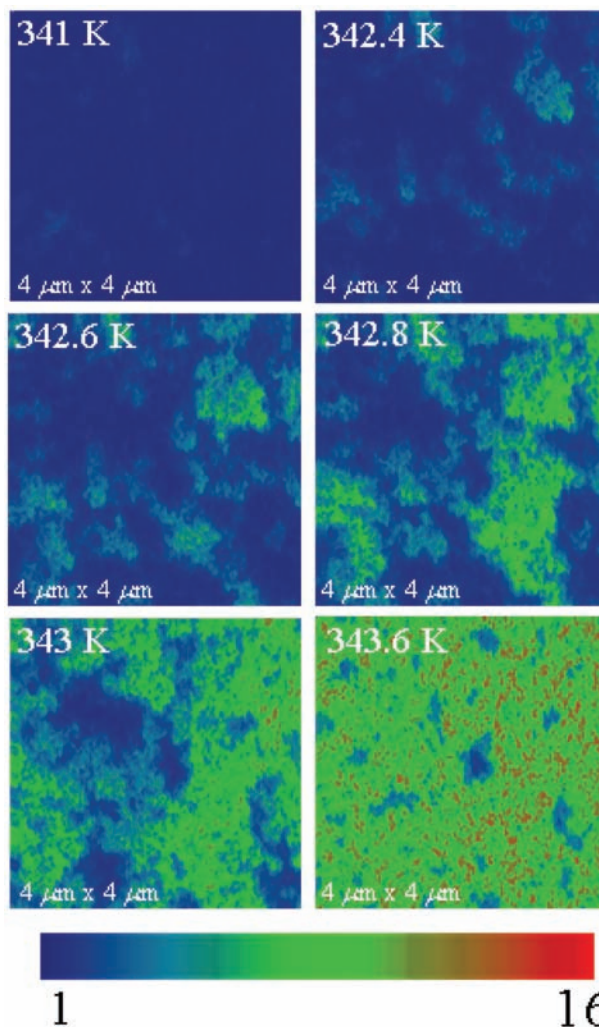


Fig. 2. Images of the near-field scattering amplitude over the same 4- μm -by-4- μm area obtained by s-SNIM operating at the infrared frequency $\omega = 930$ cm⁻¹. These images are displayed for representative temperatures in the insulator-to-metal transition regime of VO₂ to show percolation in progress. The metallic regions (light blue, green, and red colors) give higher scattering near-field amplitude compared with the insulating phase (dark blue color). See (13) for details.

¹Physics Department, University of California–San Diego, La Jolla, CA 92093, USA. ²Abt. Molekulare Strukturbiologie, Max-Planck-Institut für Biochemie and Center for NanoScience, 82152 Martinsried, München, Germany. ³IT Convergence and Components Laboratory, Electronics and Telecommunications Research Institute, Daejeon 305-350, Korea. ⁴Theoretical Division and Center for Integrated Nanotechnologies, MS B262, Los Alamos National Laboratory, Los Alamos, NM 87545, USA.

*To whom correspondence should be addressed. E-mail: mumtaz@physics.ucsd.edu

tronic mean free path of the order of the lattice constant, reminiscent of “bad metal” behavior in other transition metal oxides, including the cuprates (21–23). The insulator-to-metal transition is evident from the increase of the conductivity with spectral weight “filling up” the energy gap that has to be contrasted with a gradual decrease of the energy gap magnitude. This feature of the transition, along with an isosbestic point at a frequency of $11,500 \pm 125 \text{ cm}^{-1}$, is one of several spectroscopic fingerprints of doped Mott insulators (1) identified in this work. The isosbestic point is defined here as the location of equal conductivity for all spectra obtained at different temperatures. Lastly, the divergence of the real part of the dielectric function ϵ_1 (Fig. 1 inset) signals the percolative nature of the insulator-to-metal transition. This divergence of ϵ_1 is similar to that observed near the percolative insulator-to-metal transition in ultrathin Au and Pb films (24).

Mid-infrared near-field images directly show that in fact the insulating and metallic phases coexist in VO_2 over a finite temperature range in the transition region (Fig. 2). This determination was made by using a scattering scanning near-field infrared microscope (s-SNIM) operating at the infrared frequencies $\omega = 930 \text{ cm}^{-1}$ and $\omega = 1725 \text{ cm}^{-1}$. s-SNIM is capable of registering contrast

between electronic phases according to their optical constants with spatial resolution $\approx 20 \text{ nm}$. Specifically, the scattering amplitude signal demodulated at the second harmonic of the tapping frequency of the tip of our s-SNIM apparatus (maps in Fig. 2) is related to the local value of the complex dielectric function $\tilde{\epsilon} = \epsilon_1 + i\epsilon_2$ of the sample. The amplitude of the scattering signal is expected to increase in metallic regions compared with that in the insulating regions: a behavior grasped well by the so-called dipole model of the near-field infrared contrast (9, 10, 13).

The amplitude-contrast near-field images in Fig. 2 show the electronic insulator-to-metal transition in progress. At temperatures between 295 and 341 K in the insulating phase, we observed uniform maps of low scattering (dark blue color in Fig. 2). A small increase of temperature radically changes the near-field images. For example, in the $T = 342.4 \text{ K}$ image we then observed nanoscale clusters in which the amplitude of the scattering signal was enhanced by a factor of 2 to 5 compared with that of the insulating host, indicating a metallic phase. Representative scans showed that the metallic regions nucleate, then grow with increasing temperature, and eventually connect. We did not observe any obvious correlations between the size and/or shape of the metallic clusters and the

features in simultaneously collected topographic images. Although the percolative nature of the insulator-to-metal transition had been proposed previously (25), it is directly revealed by our scanning near-field infrared measurements reported herein. The insulator-to-metal transition is complete by $T = 360 \text{ K}$, at which temperature insulating islands are no longer seen.

With the observation of nanostructured phases in Fig. 2, the far-field infrared spectra in Fig. 1 should be analyzed with use of an effective medium theory (EMT) for such phase-separated systems (13, 26). The effective optical constants of a two-phase heterogeneous system are an average of the optical constants of the insulating and metallic regions weighted by the respective volume fractions. Our near-field images enabled us to determine these fractions. However, a simple weighting of optical constants of the insulating phase and of the rutile metallic phase at $T = 360 \text{ K}$ within the EMT model does not produce a satisfactory description of the far-field infrared data near the onset of the insulator-to-metal transition in VO_2 . This discrepancy indicates that the infrared properties of the metallic puddles, once they first appear at $T \approx 342 \text{ K}$, may be different from that of the high-temperature rutile metal. We confirmed this hypothesis by extracting the response of the metallic puddles from a combi-

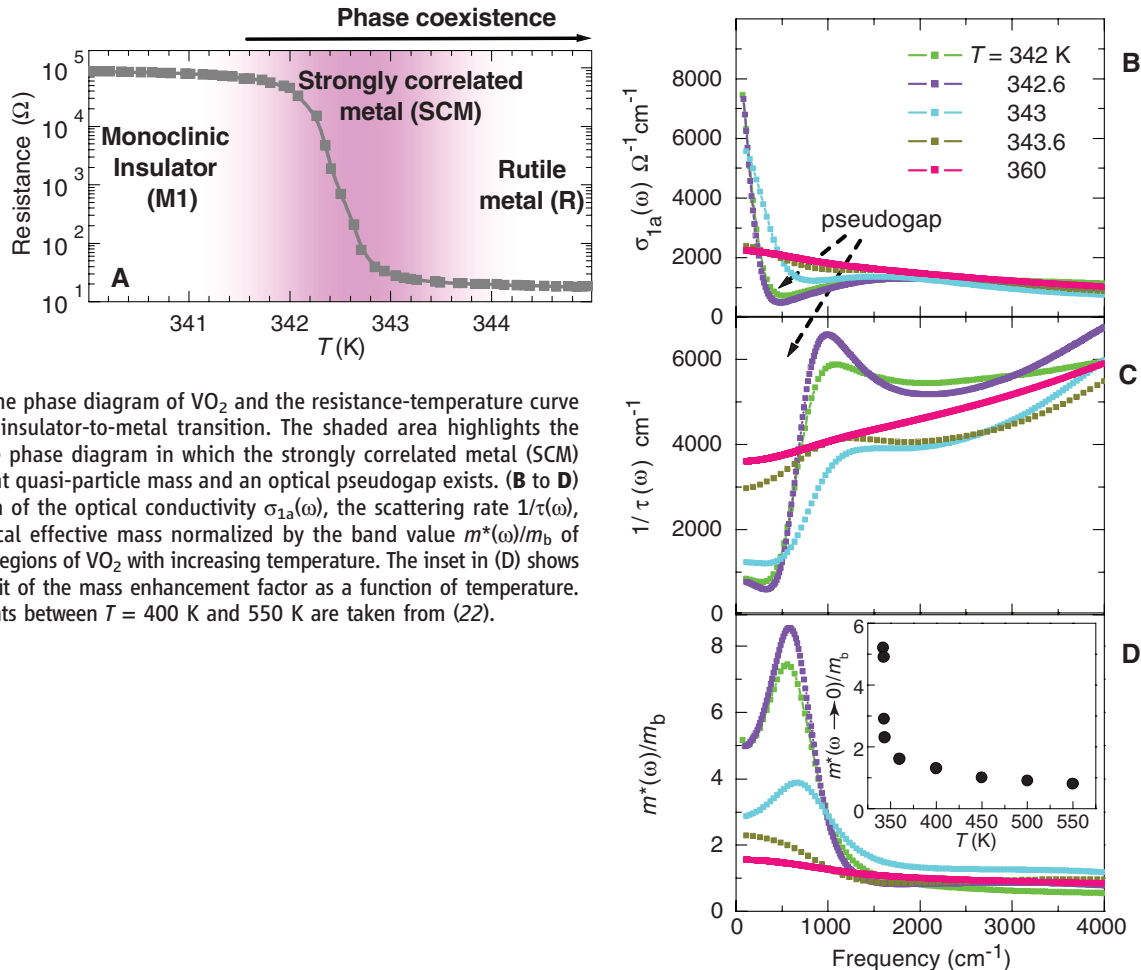


Fig. 3. (A) The phase diagram of VO_2 and the resistance-temperature curve showing the insulator-to-metal transition. The shaded area highlights the region of the phase diagram in which the strongly correlated metal (SCM) with divergent quasi-particle mass and an optical pseudogap exists. (B to D) The evolution of the optical conductivity $\sigma_{1a}(\omega)$, the scattering rate $1/\tau(\omega)$, and the optical effective mass normalized by the band value $m^*(\omega)/m_b$ of the metallic regions of VO_2 with increasing temperature. The inset in (D) shows the $\omega \rightarrow 0$ limit of the mass enhancement factor as a function of temperature. The data points between $T = 400 \text{ K}$ and 550 K are taken from (22).

nation of near-field results and far-field spectra within an EMT analysis described in (13).

The real part of the conductivity spectrum, $\sigma_{1a}(\omega)$, of the metallic puddles is plotted in Fig. 3B as it evolves with temperature. When these puddles appear at the onset of the electronic insulator-to-metal transition at $T \approx 342$ K (Fig. 3A), their conductivity spectrum differs markedly from that of the rutile metallic phase at higher temperature, for example, $T = 360$ K. These metallic regions exhibit a narrow Drude-like peak at low frequencies and then a dip, followed by a prominent mid-infrared band that peaked at ≈ 1800 cm^{-1} . Uncertainties in the EMT analysis [detailed in (13)] do not exclude the possibility of a nonmonotonic form of $\sigma_{1a}(\omega)$ at the lowest frequencies, a behavior consistent with Drude response modified by localization. These features indicate that the metallic islands are not simply isolated regions of the higher-temperature VO_2 rutile metal.

In order to highlight distinctions between the electrodynamic of the metallic clusters and the rutile metallic phase, we performed the extended Drude analysis (13, 27) on the optical constants of the metallic clusters to extract the scattering rate $1/\tau(\omega)$ and the mass enhancement factor $m^*(\omega)/m_b$ (m_b is the electronic band mass) of the charge carriers (Fig. 3, C and D). In the limit of $\omega \rightarrow 0$, these quantities can be interpreted in terms of lifetime, $\tau(\omega)$, and effective mass, $m^*(\omega)$, of quasiparticles (27) in the metallic regions. One can recognize a prominent enhancement of $m^*(\omega \rightarrow 0)/m_b$ at $T = 342$ K that has to be contrasted with much lighter masses in the rutile phase ($T = 360$ K) spectrum in Fig. 3D (22). More importantly, the temperature dependence of $m^*(\omega \rightarrow 0)/m_b$, plotted in the inset of Fig. 3D, shows divergent behavior in the vicinity of the insulator-to-metal transition: an unambiguous attribute of the Mott transition (28). The spectra of $1/\tau(\omega)$ reveal a threshold structure followed by an overshoot at higher energies up to ≈ 1000 cm^{-1} . This is characteristic of systems with a (pseudo)gap in the electronic density of states (29) that is to be contrasted with the relatively smooth variation of $1/\tau(\omega)$ in the rutile phase. We also note that the new electronic state exhibiting an enhanced mass and a gaplike form of the relaxation rate exists only in a narrow temperature range, as shown by the shaded region in Fig. 3A. By $T = 343.6$ K, the optical constants of the metallic regions already resemble those of the rutile metallic phase.

The analysis and discussion above suggest that the classic temperature-induced insulator-to-metal transition in VO_2 occurs from the monoclinic insulator to an incipient strongly correlated metal (SCM) in the form of nanoscale puddles. These metallic puddles exhibit mass divergence, which is a clear signature of electronic correlations due to many-body Coulomb interactions (28). The pseudogap and mid-infrared band are consequences of optically induced electronic excitations across a gap on some parts of the Fermi surface. The energy scale of the pseudogap in the SCM

state in VO_2 can be determined by the overshoot in $1/\tau(\omega)$ spectra that occurs at ≈ 1000 cm^{-1} (or $\approx 4k_B T_c$). We note that the pseudogap is a common property of doped Mott insulators (1, 27). The pseudogap features in the optical conductivity and $1/\tau(\omega)$ spectra also bear resemblance to those found in metallic systems with a partial charge density wave (CDW) gap (30). The pseudogap in VO_2 may result from a complex interplay between electronic correlations and charge ordering.

The Mott transition commonly leads to an antiferromagnetically ordered insulator as in closely related V_2O_3 (1). Vanadium dioxide avoids this magnetic ordering via dimerization of vanadium ions in the monoclinic insulating phase (14) because of competing effects of charge ordering (Peierls instability) that is likely caused by electron-phonon interactions. Thus, the insulating monoclinic (M1) phase of VO_2 should be classified as a Mott insulator with charge ordering. It remains an open question whether or not the insulator-to-metal transition occurs at a slightly different temperature from the structural transformation associated with charge ordering (18, 19, 31), and this raises the issue about the precise lattice structure of the metallic nanopuddles we have observed. This issue does not affect our observation of divergent optical mass and can only be resolved by x-ray diffraction measurements on the nanoscale. We also note that the images of phase coexistence and percolation reported here (Fig. 2) are consistent with the thermodynamic evidence of the first-order nature of the phase transition in VO_2 (21). Moreover, our experiments show that the collapse of a large ≈ 0.5 eV energy gap and the formation of heavy quasi-particles in the emergent metallic nanopuddles at the onset of the insulator-to-metal transition are due to Mott physics (1, 28) and that percolation occurs at a later stage when these metallic puddles grow and connect (Fig. 2).

A transformation from an insulator to a metal in many correlated electron systems, including high- T_c cuprates, colossal magnetoresistive manganites, and others, occurs through an intermediate pseudogap regime (1, 5, 27, 29). At least in the case of cuprates, optical signatures of the pseudogap state are similar to the results in the SCM state of VO_2 (27). Furthermore, in many correlated systems, the pseudogap state is in the vicinity of the regime of the bad metal in which resistivity shows a peculiar linear dependence with temperature, whereas the absolute values of the resistivity are so large that the notion of quasiparticles becomes inapplicable (21–23). Often a crossover from pseudogapped metal to bad metal occupies an extended region of the phase diagram. In VO_2 , the boundary between the two electronic regimes is relatively abrupt, and the emergence of bad metal transport in the rutile phase may be linked to the loss of long-range charge order that does not extend into the rutile metal. Then the poor conductivity of rutile VO_2 and other bad metals appears to arise from the collapse of electronically and/or magnetically or-

dered states in the vicinity of a Mott insulator, thereby causing the resistivity to exceed the Ioffe-Regel-Mott limit of metallic transport (21–23). Lastly, we note that, in the cuprates, in contrast to VO_2 , the effective mass of doped carriers inferred from infrared spectroscopy data (32) shows no divergence. However, if electronic phase separation exists in doped cuprates, as suggested by recent scanning probe studies (6, 8), then infrared analysis of the effective quasi-particle mass needs to be revisited with the help of nano-imaging tools used in this work.

References and Notes

- M. Imada, A. Fujimori, Y. Tokura, *Rev. Mod. Phys.* **70**, 1039 (1998).
- V. J. Emery, S. A. Kivelson, J. M. Tranquada, *Proc. Natl. Acad. Sci. U.S.A.* **96**, 8814 (1999).
- M. Uehara, S. Mori, C. H. Chen, S.-W. Cheong, *Nature* **399**, 560 (1999).
- L. Zhang, C. Israel, A. Biswas, R. L. Greene, A. de Lozanne, *Science* **298**, 805 (2002); published online 19 September 2002 (10.1126/science.1077346).
- E. Dagotto, *Science* **309**, 257 (2005).
- J. Lee *et al.*, *Nature* **442**, 546 (2006).
- Z. Sun *et al.*, *Nat. Phys.* **3**, 248 (2007).
- K. K. Gomes *et al.*, *Nature* **447**, 569 (2007).
- B. Knoll, F. Keilmann, *Nature* **399**, 134 (1999).
- F. Keilmann, R. Hillenbrand, *Philos. Trans. R. Soc. London Ser. A* **362**, 787 (2004).
- N. Ocelic, A. Huber, R. Hillenbrand, *App. Phys. Lett.* **89**, 101124 (2006).
- B. G. Chae *et al.*, *Electrochem. Solid-State Lett.* **9**, C12 (2006).
- See Materials and Methods on Science Online.
- R. M. Wentzcovitch, W. W. Schulz, P. B. Allen, *Phys. Rev. Lett.* **72**, 3389 (1994).
- T. M. Rice, H. Launois, J. P. Pouget, *Phys. Rev. Lett.* **73**, 3042 (1994).
- S. Biermann, A. Poteryaev, A. I. Lichtenstein, A. Georges, *Phys. Rev. Lett.* **94**, 026404 (2005).
- T. C. Koethe *et al.*, *Phys. Rev. Lett.* **97**, 116402 (2006).
- H.-T. Kim *et al.*, *Phys. Rev. Lett.* **97**, 266401 (2006).
- H.-T. Kim *et al.*, *N. J. Phys.* **6**, 52 (2004).
- E. Arcangeletti *et al.*, *Phys. Rev. Lett.* **98**, 196406 (2007).
- P. B. Allen, R. M. Wentzcovitch, W. W. Schulz, P. C. Canfield, *Phys. Rev. B* **48**, 4359 (1993).
- M. M. Qazilbash *et al.*, *Phys. Rev. B* **74**, 205118 (2006).
- V. J. Emery, S. A. Kivelson, *Phys. Rev. Lett.* **74**, 3253 (1995).
- J. J. Tu, C. C. Homes, M. Strongin, *Phys. Rev. Lett.* **90**, 017402 (2003).
- H. S. Choi, J. S. Ahn, J. H. Jung, T. W. Noh, D. H. Kim, *Phys. Rev. B* **54**, 4621 (1996).
- G. L. Carr, S. Perkowitz, D. B. Tanner, in *Infrared and Millimeter Waves*, K. J. Button, Ed. (Academic Press, Orlando, 1985), vol. 13.
- D. N. Basov, T. Timusk, *Rev. Mod. Phys.* **77**, 721 (2005).
- W. F. Brinkman, T. M. Rice, *Phys. Rev. B* **2**, 4302 (1970).
- D. N. Basov, E. J. Singley, S. V. Dordevic, *Phys. Rev. B* **65**, 054516 (2002).
- G. Gruner, *Density Waves in Solids* (Perseus Publishing, Cambridge, MA, 2000).
- Y. J. Chang *et al.*, *Phys. Rev. B* **76**, 075118 (2007).
- W. J. Padilla *et al.*, *Phys. Rev. B* **72**, 060511(R) (2005).
- This work was supported by the U.S. Department of Energy, the Deutsche Forschungsgemeinschaft Cluster of Excellence Munich-Centre for Advanced Photonics, and the Electronics and Telecommunications Research Institute (ETRI), Korea.

Supporting Online Material

www.sciencemag.org/cgi/content/full/318/5857/1750/DC1
Materials and Methods
SOM Text
Table S1

5 September 2007; accepted 31 October 2007
10.1126/science.1150124